Hyperfine Interactions **138:** 331–341, 2001.

μCF Experiments in D_2 and HD Gases – Final Results

N. I. VOROPAEV[1], D. V. BALIN[1], W. H. BREUNLICH[2], T. CASE[3], K. M. CROWE[3], M. P. FAIFMAN[5], B. GARTNER[2], F. J. HARTMANN[4], P. KAMMEL[3], B. LAUSS[2], E. M. MAEV[1], V. E. MARKUSHIN[6], C. PETITJEAN[6], G. E. PETROV[1], G. N. SCHAPKIN[1], G. G. SEMENCHUK[1], A. A. VOROBYOV[1] and J. ZMESKAL[2]

[1] *Petersburg Nuclear Physics Institute (PNPI), Gatchina 188350, Russia*
[2] *Institute for Medium Energy Physics (IMEP), A-1090 Wien, Austria*
[3] *University of California Berkeley, UCB and LBNL, Berkeley, CA 94720, USA*
[4] *Technical University of Münich (TUM), D-85747 Garching, Germany*
[5] *Russian Research Centre "Kurchatov Institute", Moscow 123182, Russia*
[6] *Paul Scherrer Institute, PSI, CH-5232 Villigen, Switzerland*

Abstract. During 1994–1996, a series of μCF experiments were performed at PSI by the PSI-PNPI-IMEP-LBNL-TUM collaboration. These experiments aimed at high-precision studies of the d–μ–d fusion in D_2 and HD gases in a wide temperature range. The Gatchina ionization time projection chamber has been used to detect the dd-fusion reaction products. The main parameters of the d–μ–d fusion have been measured with high absolute precision. In this report, we present the results of the final analysis of the experimental data. The obtained results are compared with the calculations based on a recent μCF-theory.

1. Introduction

After the experimental discovery of resonant mechanism of ddμ molecule formation [1], due to the "Vesman mechanism" [2], muon catalyzed dd-fusion was the subject of numerous investigations, see reviews [3, 4]. The agreement reached with the theory was quite impressive [5], still the method using the high-pressure ionization chamber from Gatchina allows to investigate and test a number of ddμ problems on a qualitatively new level of accuracy $\sim$1%. This experimental method was described in [6–10] and was presented at this meeting too. Here we shall point out only the main features of the method. The high pressure hydrogen ionization chamber (IC) was used as an active target. It allowed to determine clean muon stops in the sensitive IC volume, well separated in space from the IC electrodes. The IC has the capability to detect with 100% efficiency all charged products of the dd-fusion reaction and to separate all the channels of this reaction

$$dd\mu \rightarrow \begin{cases} {}^3\mathrm{He} + \mathrm{n} + \mu, \\ {}^3\mathrm{He}\mu + \mathrm{n}, \\ \mathrm{t} + \mathrm{p} + \mu\ . \end{cases}$$

We have measured the d–μ–d fusion observables with an absolute precision up to 1%. The IC could operate in a wide temperature range from 28 to 350 K, the temperature being determined for each data point to absolute precision of ± 0.15 K. The IC was filled with pure D_2 or with $H_2 + D_2$ gas mixture. Also, measurements were performed with a specially prepared pure HD gas where admixture of D_2 molecules was only on a level of 1%. The IC was surrounded with an array of scintillator counters for detection of neutrons from the fusion reaction. The main (though small) background in these studies was due to muon capture on the hydrogen contamination with N_2, O_2, H_2O on a level a few ppm. However, the IC allowed to detect directly the products of the muon capture reactions and to subtract this background in the analysis of the experimental data. Preliminary results of these measurements were published in [11–13].

2. Analysis and results

Below we present the results of analysis of the experimental runs performed at various temperatures with pure D_2 gas (17 runs), with equilibrated $H_2 + HD + D_2$ (4 runs) and non-equilibrated $H_2 + D_2$ (3 runs) gas mixture, and also with HD gas (3 runs).

For analysis, only those events were selected with the muon stops in the sensitive volume of the IC, well separated in space from the IC electrodes and from the walls. This selection was done using the values of amplitude and time of the muon signals in the IC. Typically, around $3 \cdot 10^6$ clean muon stops were selected from 10^7 events in each run, and amplitude and time distributions of the fusion signals were analyzed. As an example, Figure 1 presents such distributions measured in pure D_2 at 120.3 K. In the amplitude spectrum, one can see the peaks corresponding to the dd-fusion channels with ^{3}He + n, ^{3}Heμ + n, and t + p in the final state. The separation of the ^{3}He and ^{3}Heμ peaks is due to difference in recombination of the primary ionization produced by the $^3He^{++}$ and $^3He\mu^+$ particles (initial energy around 0.8 MeV). The continuous spectrum of the t + p channel is a result of the probability for the long range protons ($E_p = 3.02$ MeV) to escape from the sensitive volume of the IC. The time distribution exhibits a typical two-exponential decay. The fast component corresponds to the ddμ formation from the upper 3/2-state of the dμ-atom. The slow component corresponds to the thermal steady equilibrium state between the lower and the upper states of the dμ-atom where the ddμ formation occurs predominantly from the lower 1/2-state. The steady state amplitude distribution is shown in Figure 2(a).

Analysis of the experimental data was performed using the kinetics scheme shown in Figure 2(b). In the first step the background was subtracted consisting mainly from muon capture reactions on gas impurities (mostly N_2). A special run was carried out with a H_2+N_2 (140 ppm) gas mixture, allowing to measure the amplitude distribution of the μ-capture events. The time distribution of the μ-capture events $Y_c(t)$ was measured in a D_2 run at 50.2 K which contained the highest level

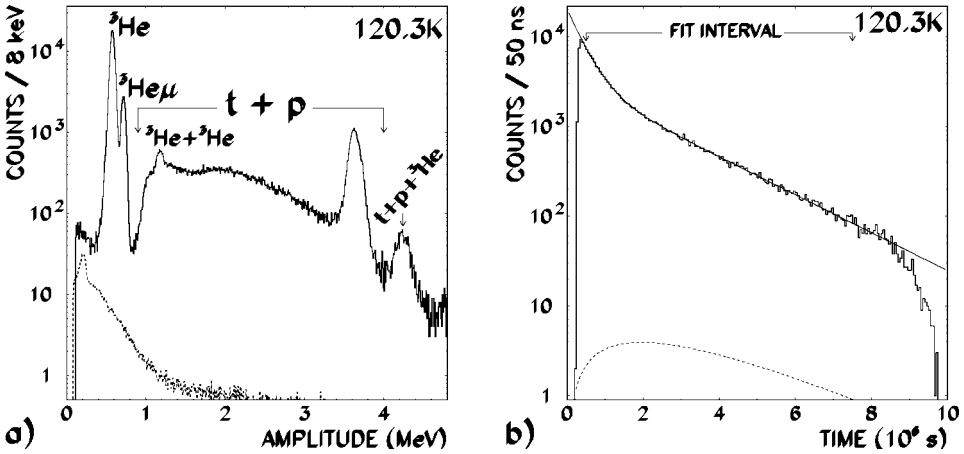

Figure 1. (a) Amplitude spectrum of fusion signals from the IC in D_2 gas. The dashed line corresponds to muon capture background. (b) Time distribution of ^{3}He and ^{3}Heμ signals. The dashed line corresponds to the μ-capture background. Solid line is the result of the kinetic fit.

of impurities. In these measurements, an amplitude interval $(0.1 \div 0.45)$ MeV was selected, where the μ-capture events dominate. The measured $Y_c(t)$ distribution allowed to determine the muon transfer rate to heavy admixture Λ_Z and the detection efficiency for the μ-capture events $w_r = 0.55(3)$. In addition, the muon capture rate was found to be: $\lambda_c = 0.057(6)\ \mu s^{-1}$ that turned out to be equal to the known value of the μ-capture rate on nitrogen. It was possible to determine the μ-capture background in each run by normalizing the μ-capture amplitude distribution to the d–μ–d fusion ones in the region $(0.1 \div 0.45)$ MeV, where μ-capture events dominate (Figure 2(a)). Note that the steady-state region was used for this fit to exclude distortion of the low-energy part of the spectrum by signals of double muons (Figure 1(a)). Such normalization, together with the measured values for λ_c and w_r, allowed to determine the transfer rate $\Lambda_z = \lambda_z \cdot C_z \cdot \phi$ in each temperature point and, using the known value $\lambda_z = 5 \cdot 10^{10}\ s^{-1}$, to find the impurity concentration C_z. Both values are presented in Tables I–III. In the particular case of D_2 at 120.3 K, $C_z = 1$ ppm the μ-capture background was very small (see Figure 1). It became more important for higher levels of impurities and for lower dd-fusion rates. However, in all cases this capture background was under control and could not deteriorate the analysis precision. Other sources of background (double muon events, etc.) were negligible. This was checked in a run with μ^+ beam under the same intensity and energy of muons.

2.1. ddμ-MOLECULE FORMATION AND SPIN-FLIP PROCESSES

From the analysis of the time distributions of the first ^{3}He and ^{3}Heμ signals (Figure 1(b)), one can determine the ddμ-molecule formation rates $\Lambda_{dd\mu}^{3/2} = \lambda_{dd\mu}^{3/2} \cdot C_d \cdot \phi$ and $\Lambda_{dd\mu}^{1/2} = \lambda_{dd\mu}^{1/2} \cdot C_d \cdot \phi$ from the $F = 3/2$ and $F = 1/2$ hyperfine states, respec-

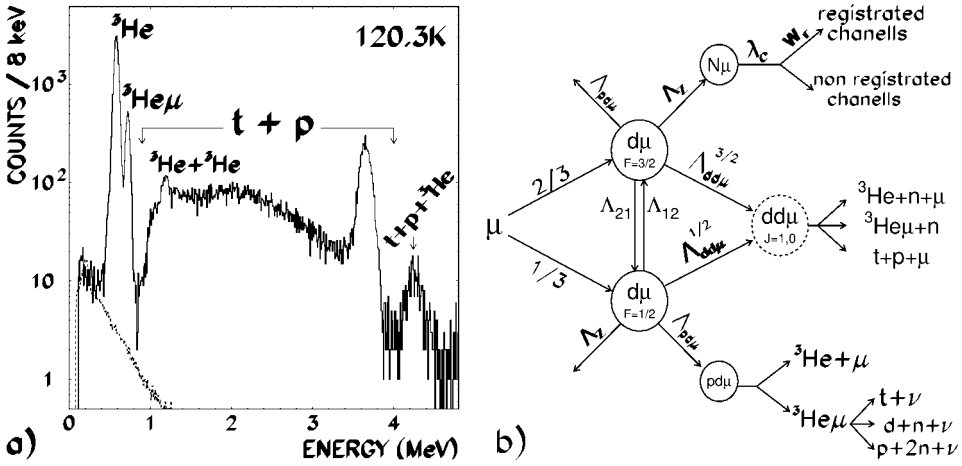

Figure 2. (a) Amplitude spectrum of dd-fusion signals for steady-state time region ($t > 2$ μs). (b) Scheme of μCF kinetics used for data analysis.

tively, and also the spin transfer rate $\Lambda_{21} = \lambda_{21} \cdot C_d \cdot \phi$ from the $F = 3/2$ to $F = 1/2$ dμ-states. Here, ϕ is the normalized gas density, and λ_{21}, $\lambda_{dd\mu}^{3/2}$, $\lambda_{dd\mu}^{1/2}$ are the rates normalized to LHD ($\phi = 1$), C_d is the deuterium atomic concentration. The time distribution of the ^{3}He events was used in the fits for the following reasons:

1. The short tracks of the ^{3}He particles lead to minimal dead time and smearing.
2. Pileup probabilities of a next fusion signal on muon or on ^{3}He signal are similar due to similar pulse durations, therefore the ratio $N(^3\text{He})/N_\mu$ is measured without distortion.
3. There is the possibility of precise (± 1 ns) measurements of the actual beginning ($t = 0$) of experimental ^{3}He time distributions by analysing the time distributions of the dd-fusion neutrons detected by the scintillation counter array in coincidence with the ^{3}He IC signals.

For quantitative analysis, the kinetics scheme in Figure 2(b) was used, and the following analytical solution for the time distribution of the first ^{3}He signals was applied:

$$N_{\text{He}}(t) = N_\mu \cdot (E_1 \cdot \mathrm{e}^{K_1 \cdot t} + E_2 \cdot \mathrm{e}^{K_2 \cdot t}). \tag{1}$$

Here, E_1, K_1, E_2, K_2 are known functions expressed via three rates [6], $\lambda_{dd\mu}^{3/2}$, $\lambda_{dd\mu}^{1/2}$, λ_{21}, while the forth rate λ_{12} entering the kinetics scheme is determined by the balance equation:

$$\begin{aligned} &\lambda_{12} = \gamma \cdot \lambda_{21}, \\ &\gamma = 2 \cdot \mathrm{e}^{-\Delta/(kT)}, \quad \Delta = 0.0485 \text{ eV}, \quad k = 8.6174 \cdot 10^{-5} \text{ eV/K}. \end{aligned} \tag{2}$$

The ^{3}He time distributions were fitted with the function $Y(t) = N_{\text{He}}(t) + Y_c(t)$, where $Y_c(t)$ is the μ-capture background described above. From these fits, three parameters, $\lambda_{dd\mu}^{3/2}$, $\lambda_{dd\mu}^{1/2}$, λ_{21} were determined, (see Tables I and II, and Figure 3).

Table I. Experimental conditions and results of kinetic fits of the rates of μCF processes in pure D_2 gas

T K	ϕ %	$\lambda_{dd\mu}^{1/2}$ 10^6 s^{-1}	$\lambda_{dd\mu}^{3/2}$ 10^6 s^{-1}	λ_{21} 10^6 s^{-1}	R	Λ_z 10^6 s^{-1}	C_z 10^{-6}
28.3	2.76	0.053(3)	3.98(5)	37.0(4)	1.026	0.0002	0.14
32.2	5.14	0.051(1)	4.13(7)	37.1(3)	1.07(3)	0.003	1.2
36.2	5.14	0.049(2)	3.96(6)	36.6(2)	–	0.035	13.6
40.3	5.14	0.050(fix.)	3.88(6)	36.6(2)	–	0.063	24.5
45.3	5.05	0.0515(8)	3.92(6)	36.8(3)	1.03(3)	0.0003	0.12
50.2	5.13	0.0544(fix.)	3.90(6)	35.9(3)	–	0.116	45.2
51.0	5.05	0.0537(7)	3.79(4)	35.77(16)	1.05(1)	0.0056	2.2
60.3	5.04	0.063(1)	3.89(6)	36.04(25)	1.08(2)	0.00053	0.21
71.0	5.04	0.088(1)	4.05(5)	35.38(25)	1.24(1)	0.0054	2.2
96.0	5.02	0.246(3)	4.42(7)	34.8(4)	1.34(1)	0.0057	2.3
120.3	4.99	0.528(4)	4.98(10)	35.0(5)	1.40(1)	0.0024	1.0
150.3	4.97	0.943(5)	5.07(15)	35.9(9)	1.43(1)	0.0034	1.4
200.2	4.94	1.65(2)	4.59(15)	34.2(1.5)	1.40(1)	0.004	1.6
250.1	4.89	2.202(27)	4.28(12)	37.0(2.0)	1.42(1)	0.007	2.9
300.0	4.85	2.549(23)	3.75(fix.)	–	1.44(1)	0.012(2)	4.9
350.0	4.81	2.70(5)	3.28(fix.)	–	1.44(1)	0.093(2)	39.0

Qualitatively, the parameters $\lambda_{dd\mu}^{3/2}$, $\lambda_{dd\mu}^{1/2}$, λ_{21} are determined by the amplitude of the fast exponent at $t = 0$, by the amplitude of the slow exponent at $t = 0$, and by the slope of the fast exponent, respectively. Note that in D_2 gas at higher temperature points (300 and 350 K) only one exponent was observed in the time distributions of the ^{3}He signals. Separation of $\lambda_{dd\mu}^{3/2}$ and $\lambda_{dd\mu}^{1/2}$ in these runs was not possible. It was possible only to determine one parameter, the rate $\lambda_{dd\mu}$ of the ddμ-molecule formation for the steadystate population of the hyperfine states of the dμ-atoms. In Table I we present the values of $\lambda_{dd\mu}^{1/2}$ at 300 K and 350 K recalculated from the measured values of $\lambda_{dd\mu}$, with the values for $\lambda_{dd\mu}^{3/2}$ fixed to the theoretical expectations (solid curves of Figure 3(a)) using the equation:

$$\lambda_{dd\mu}(T) = \frac{1}{1+\gamma} \cdot \lambda_{dd\mu}^{1/2}(T) + \frac{\gamma}{1+\gamma} \cdot \lambda_{dd\mu}^{3/2}(T). \tag{3}$$

In the $H_2(50\%) + D_2(50\%)$ runs, the separation of $\lambda_{dd\mu}^{3/2}$ and $\lambda_{dd\mu}^{1/2}$ was possible even at 300 K due to a twofold lower spin-flip rate (Table II).

The temperature dependence of $\lambda_{dd\mu}^{3/2}(T)$ and $\lambda_{dd\mu}^{1/2}(T)$ (see Figure 3(a)) demonstrates a remarkable resonance behaviour of the ddμ-molecule formation rates. Only at low temperatures $T \leqslant 50$ K, the ddμ-formation from the $F = 1/2$ dμ-state is non-resonant. The non-resonant mechanism gives the main contribution

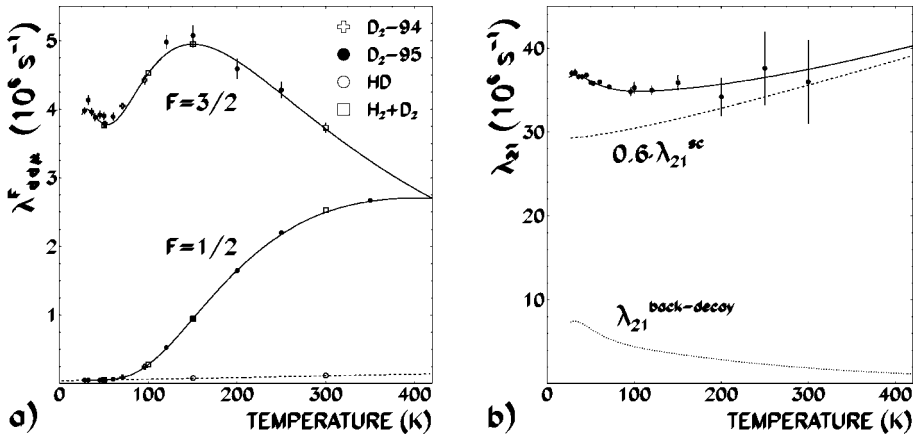

Figure 3. (a) Absolute rates for ddμ formation versus temperature in D_2 and in H/D gas mixtures. The curves present the fit by the theory. (b) Spin-flip rates on D_2 molecules. Full curve: fit of the experimental data by superposition of the two theoretical curves (dashed and dotted lines) after renormalisation of the non-resonant curve.

to the ddμ-formation on the HD molecules in the whole investigated temperature range. The HD runs were performed with the goal to study the non-resonant ddμ-formation process, while the resonant one is suppressed [14]. The main problem of this experiment was elimination of D_2 from the HD gas as the ddμ formation rate on D_2 is by a factor of 20 larger than on HD (at $T = 300$ K). Using a specially developed method [15], we prepared very clean HD gas containing only $\sim$1% of D_2 molecules. Still the background due to dd-fusion on D_2 molecules was considerable. It was separated by observing the fast exponent in the time spectra. In this way, the C_{D_2} concentration was determined, and it proved to be in good agreement with the chromatographic analysis of the gas (Table III).

In the fits of the ^{3}He time distributions, we assumed that the rates of the ddμ formation on HD $\lambda_{dd\mu}^{HD}$ are equal for both dμ spin states. The results of the fits are presented in Table III and in Figure 3(a). The observed $\lambda_{dd\mu}^{HD}(T)$ shows a weak linear dependence with temperature:

$$\lambda_{dd\mu}^{HD}(T) = (2.4 \cdot 10^{-4} \cdot T + 0.041)\ \mu s^{-1}. \tag{4}$$

Such a dependence is in qualitative agreement with the theoretical prediction for non-resonant ddμ formation rates [16]:

$$\lambda_{dd\mu}^{nr}(T) = (2.4 \cdot 10^{-4} \cdot T + 0.027)\ \mu s^{-1}. \tag{5}$$

2.2. TEMPERATURE DEPENDENCE OF THE SPIN-FLIP RATE $\lambda_{21}(T)$

The dμ spin-flip rate contains two components. One is direct spin transfer $(d\mu)_{F=3/2} \rightarrow (d\mu)_{F=1/2}$ in the non-resonant scattering of the dμ atoms on D_2

Table II. Experimental conditions and results of kinetic fits of the rates of μCF processes in $H_2(50\%) + D_2(50\%)$ gas mixture. EQ – equilibrium and NE – non-equilibrium mixtures

T K	Gas mixture state	ϕ %	$\lambda_{dd\mu}^{1/2}$ 10^6 s^{-1}	$\lambda_{dd\mu}^{3/2}$ 10^6 s^{-1}	λ_{21} 10^6 s^{-1}	Λ_z 10^6 s^{-1}	C_z 10^{-6}
50	EQ	5.07	0.058(4)	3.66(3)	34.0(4)	0.0032(6)	1.3
50	NE	5.12	0.051(4)	3.74(3)	35.5(3)	0.0053(6)	2.1
100	EQ	5.00	0.279(8)	4.50(5)	33.9(5)	0.0035(10)	1.4
150	EQ	4.97	0.95(1)	4.88(5)	35.6(7)	0.0036(6)	1.4
150	NE	5.02	0.934(10)	4.94(6)	35.5(7)	0.004(1)	1.5
300	EQ	4.91	2.55(6)	3.62(18)	52(10)	0.0043(9)	1.6
300	NE	4.97	2.51(3)	3.70(7)	35(5)	0.0040(10)	1.5

Table III. Experimental conditions and results of kinetic fits of the rates of μCF processes in HD gas. C_{D_2} and $C_{D_2}^{chr}$ are the values of the concentrations of D_2 molecules obtained by fit of ^{3}He time distributions and by chromotographic analysis, respectively

T K	ϕ %	$\lambda_{dd\mu}^{HD}$ 10^6 s^{-1}	R	C_{D_2} %	$C_{D_2}^{chr}$ %	Λ_z 10^6 s^{-1}	C_z 10^{-6}
50	4.74	0.0561(8)	0.99(2)	1.16(3)	1.10	0.0043	1.7
150	4.78	0.0801(24)	1.01(2)	1.06(5)	1.02	0.0027	1.3
300	4.87	0.119(6)	1.00(2)	0.82(8)	0.78	0.0032	1.5

molecules with rate $\lambda_{21}^{sc}(T)$. The second one is the contribution $\lambda_{21}^{bd}(T)$ to spin-flip via back-decay of the ddμ-molecule. The theory [14, 17] predicts significantly different shapes of the temperature dependences of these two rates (Figure 3(b)) allowing to separate the two components in fitting to the measured $\lambda_{21}(T)$ by the sum:

$$\lambda_{21}(T) = \alpha \cdot \lambda_{21}^{bd}(T) + \beta \cdot \lambda_{21}^{sc}(T). \tag{6}$$

Here α and β are the normalization factors to be found from the fit, the temperature dependences of the two components being taken from the theory. This procedure can reproduce the experimental data on $\lambda_{21}(T)$ (see Figure 3(b)) only when the theoretical function $\lambda_{21}^{sc}(T)$ is renomalized by a factor 0.6, while the back-decay rate can be kept close to the theoretical prediction ($\alpha \approx 1$). The disagreement with the theory of $\lambda_{21}^{sc}(T)$ needs theoretical explanation.

Table IV. World results of measured and predicted dd fusion branching ratios

$R_{J=0}$	$R_{J=1}$	Comments
0.886	1.43	Coulomb-corrected R-matrix calculation [19]
0.902(5)	1.459(16)	phase-shift analysis of the exp. data [18]
0.901(12)	1.450(11)	direct measurement (this work)

2.3. BRANCHING RATIO OF dd-FUSION CHANNELS

The branching ratio of the dd-fusion channels, $R = N(^3\mathrm{He} + \mathrm{n})/N(\mathrm{t} + \mathrm{p})$, was measured in the D_2 and HD runs using the amplitude distribution for the steady state region (Figure 2(a)). It was determined by the ratio of the number of events in the energy range $(0.45 \div 0.90)$ MeV to that in the energy range $(0.90 \div 4.0)$ MeV. Only one correction for the pileup of the next fusion on the ^{3}He signal was applied. As a result, the ratio R was determined with a precision of $(1 \div 3)\%$. The results are presented in Tables I and III and in Figure 4(a). In the case of d–μ–d fusion in D_2 gas, a strong temperature dependence of $R(T)$ is seen. On the other hand, $R(T) \sim$ constant in the case of d–μ–d fusion in the HD gas. The following expression was used to fit the experimental points:

$$R(T) = \frac{(\lambda_{\mathrm{dd}\mu}(T) - \lambda_{\mathrm{dd}\mu}^{\mathrm{nr},J=0}(T)) \cdot R_{J=1} + \lambda_{\mathrm{dd}\mu}^{\mathrm{nr},J=0}(T) \cdot R_{J=0}}{\lambda_{\mathrm{dd}\mu}(T)}. \tag{7}$$

Here, J is the total orbital momentum of the ddμ molecule, $R_{J=1}$ and $R_{J=0}$ are free parameters, $\lambda_{\mathrm{dd}\mu}(\mathrm{T})$ is the steady-state ddμ formation rate determined by Equation (3), $\lambda_{\mathrm{dd}\mu}^{\mathrm{nr},J=0}(T) = \lambda_{\mathrm{dd}\mu}^{\mathrm{HD}}(\mathrm{exp.}) - \lambda_{\mathrm{dd}\mu}^{\mathrm{nr},J=1}(\mathrm{theor.})$, where $\lambda_{\mathrm{dd}\mu}^{\mathrm{nr},J=1}(\mathrm{theor.}) = 0.012\ \mu\mathrm{s}^{-1}$ [16]. The fit results are presented in Table IV. Strong isotopic asymmetry of dd-fusion is seen in the $J = 1$ ddμ-state where the fusion occurs in the P-wave of the dd-system. Similar effect was observed in the phase-shift analysis of the dd-scattering data [18]. Recently, this asymmetry was reproduced by a theory based on the Coulomb-corrected R-matrix calculations [19].

2.4. MUON STICKING PROBABILITY

The effective muon sticking probability ω_d was determined from the ratio of the number of events in the ^{3}Heμ peak to that in both the ^{3}He and ^{3}Heμ peaks in the amplitude distribution of the dd-fusion signals: $\omega_d = N(^3\mathrm{He}\mu)/N(^3\mathrm{He} + {}^3\mathrm{He}\mu)$. To determine $N(^3\mathrm{He}\mu)$, an additional amplitude spectrum was compiled with the requirement of the first fusion to be followed by a second one ("survived muon method" [7]). This spectrum, normalized to the ^{3}He peak, is presented in Figure 4(b) by the dotted line. The difference between these two spectra in the

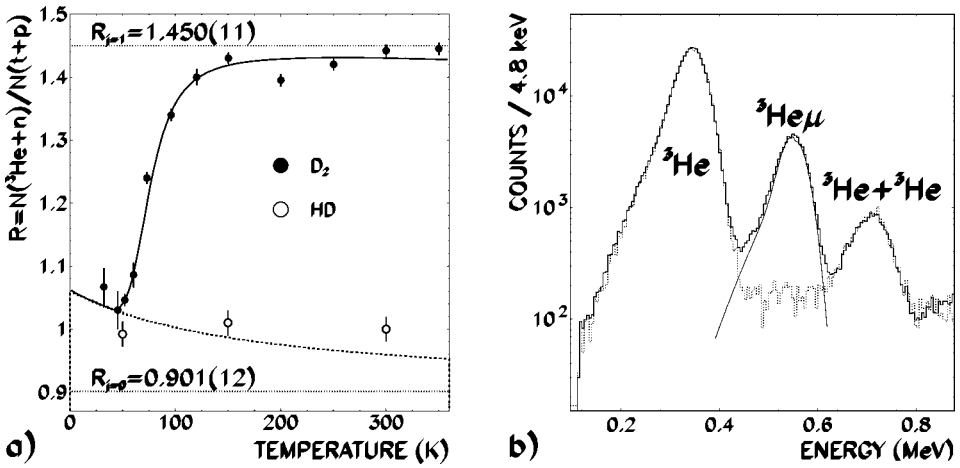

Figure 4. (a) dd-fusion branching ratio $R = N(^3\mathrm{He} + \mathrm{n})/N(\mathrm{t} + \mathrm{p})$ in D_2 and in HD gases, plotted versus gas temperature. The lines are the results of the fit with Equation (7). The dashed line corresponds to $R(T)$ of the non-resonant ddμ formation. (b) Amplitude spectra of fusion signals from the IC at $T = 300$ K and $\phi = 0.0837$ in pure deuterium corresponding to the ^{3}He channel. The dotted line shows the spectrum evaluated by the "survived muon method", where sticking events are absent. The remained spectrum in this region consists mainly of stripped events where the muon was shaken off from $^3\mathrm{He}\mu$ [20].

region of the $^3\mathrm{He}\mu$ peak gives the number $N(^3\mathrm{He}\mu)$ with high precision. Only one small correction for the pileup of the next fusion on the ^{3}He signal was applied. The results of the measurements at two deuterium densities are:

$$\omega_d(\phi = 0.0837) = 0.1206(6), \qquad \omega_d(\phi = 0.0485) = 0.1205(7)$$

with mainly statistical errors. These results can be compared with the recent theoretical calculations: $\omega_d^{\mathrm{th}} = 0.122$ [21].

3. Comparison of the measured rates with μCF theory

The temperature dependences $\lambda_{\mathrm{dd}\mu}^{3/2}(T)$, $\lambda_{\mathrm{dd}\mu}^{1/2}(T)$, and $\lambda_{21}(T)$ presented above were fitted by the theoretical distributions [14, 22] simultaneously, with a set of basic theoretical parameters left free in the fit. The comparison of the obtained parameters with the theoretical values is a sensitive test of the μCF theory. Table V demonstrates such a comparison. One can see from Figure 3(a) the very good quality of the fit. In particular, this fit allowed to extract the energy ε_{11} of the loosely bound level in the ddμ-molecule with a precision of ± 0.3 meV. This value is only by 2 meV different from the theoretical value. Note that even the vacuum polarization contribution to ε_{11} is about 10 meV. The other parameters listed in Table V proved to be also close to the theoretical values except some renormalization needed for $\lambda_{21}^{\mathrm{sc}}(T)$, parameter β.

Table V. Fit values of theoretical parameters extracted from the measured rates $\lambda_{dd\mu}^{3/2}(T)$, $\lambda_{dd\mu}^{1/2}(T)$, and $\lambda_{21}(T)$. "s.f." means scaling factor

Parameter	Fit value	Theory	Comments
ϵ_{11}	$-1.9626(3)$	-1.9648	loosely bound energy level (eV) in ddμ molecule [4]
$\lambda_f^{J=1}$	407(20)	460	effective dd fusion rate (10^6 s^{-1}) in $(dd\mu)_{J=1}^{v=1}$ state [22, 23]
$C_{\Delta F}$	1.021(3)	1.00	s.f. for dμ hfs splitting energy [24]
$C_{\Delta S}$	0.999(9)	1.00	s.f. for the ddμ hfs splitting energy [24]
C_{KI}	1.01(6)	1.00	s.f. of the rotational energy levels for the D_2 molecule [25]
C_{KF}	0.754(60)	1.00	s.f. of rotational energy levels for the ddμdee complex [25]
C_{matr}	0.746(20)	1.00	s.f. of matrix elements [22, 14]
β	0.60(1)	1.00	s.f. of non-resonant spin-flip rate [17]

4. Summary

The new experimental method developed originally at PNPI, the high pressure hydrogen time projection chamber, combined with the unique quality of the μE4 muon beam at PSI, allowed to carry out a detailed study of muon catalyzed dd-fusion in D_2, $H_2 + D_2$, and HD gases. The main parameters of the μCF processes have been measured in a wide temperature range from $T = 28$ K to $T = 350$ K with high absolute precision, namely: resonant and non-resonant ddμ-molecule formation rates; direct and back-decay spin-flip rates in the dμ-atom; branching ratios of the dd-fusion channels; muon sticking probability.

The resulting data were analyzed using the μCF theory that allowed to check several most important theoretical parameters. In particular, the energy ε_{11} of the losely bound level in the ddμ-molecule was determined with unprecedent absolute accuracy of ± 0.3 meV. The general agreement of the experiment with the theory was found to be good, with only one exception: the experimental direct spin-flip rate $\lambda_{21}^{sc}(T)$ is significantly lower than the theoretical prediction.

Acknowledgements

This work was supported in part by the Russian Foundation of Fundamental Research, grant No 00-15-96813, by the Russian Ministry of Sciences and Technology, and by the Paul Scherrer Institute. The authors thank Prof. L. I. Ponomarev for permanent interest to this work and discussions.

References

1. Dzhelepov, V. P. *et al.*, *Soviet. Phys. JETP* **19** (1964), 1376 and **23** (1966), 820.
2. Vesman, E. A., *Soviet. Phys. JETP* **5**, (1967), 9.

3. Breunlich, W. H. *et al.*, *Ann. Rev. Nucl. Part. Sci.* **39** (1989), 311; Ponomarev, L. I., *Contemp. Phys.* **31** (1991), 219; Petitjean, C., *Nucl. Phys. A* **543** (1992), 79; Kammel, P., In: L. Schaller and C. Petitjean (eds), *Muonic Atoms and Molecules*, Birkhäuser, Basel, 1993, p. 111.
4. Ponomarev, L. I., *Hyp. Interact.*, this issue.
5. Scrinzi, A. *et al.*, *Phys. Rev. A* **47** (1993), 4691.
6. Balin, D. V. *et al.*, *MCF* **5/6** (1990/91), 163.
7. Balin, D. V. *et al.*, *MCF* **7** (1992), 1.
8. Petitjean, C. *et al.*, *Hyp. Interact.* **101/102** (1996), 1.
9. Semenchuk, G. G. *et al.*, *Hyp. Interact.* **101/102** (1996), 547.
10. Ackerbauer, P. *et al.*, *Phys. Lett. B* **417** (1998), 224; Voropaev, N. I. *et al.*, Thesis, Russia PNPI Gatchina, 1998.
11. Petitjean, C. *et al.*, *Hyp. Interact.* **118** (1999), 127.
12. Voropaev, N. I. *et al.*, *Hyp. Interact.* **118** (1999), 135.
13. Semenchuk, G. G. *et al.*, *Hyp. Interact.* **118** (1999), 141.
14. Faifman, M. P., Men'shikov, L. I. and Strizh, T. A., *MCF* **4** (1988), 1; Faifman, M. P. *et al.*, *Hyp. Interact.* **101/102** (1996), 179.
15. Schapkin, G. N. *et al.*, preprint PNPI-2395, RAN, Gatchina, 2000.
16. Faifman, M. P., *MCF* **4** (1989), 341.
17. Adamczak, A. *et al.*, *Atomic Data and Nuclear Data Tables* **62**(2) (1996), 315, 329.
18. Adyasevich, B. P., Antonenko, V. G. and Fomenko, D. E., *Yad. Fiz.* **33** (1981), 1167.
19. Hale, G. M., *Muon Cat. Fusion* **5/6** (1990/91), 227.
20. Case, T. *et al.*, *Hyp. Interact.* **118** (1999), 197.
21. Men'shikov, L. I. and Ponomarev, L. I., *JETP Lett.* **41** (1985), 623.
22. Men'shikov, L. I. *et al.*, *Sov. Phys. JETP* **65** (1987), 656.
23. Bogdanova, L. N. *et al.*, *Phys. Lett.* **115B** (1982), 171; *Errata* **167B** (1986), 485.
24. Bakalov, D., *MCF* **3** (1988), 321.
25. Faifman, M. P. *et al.*, *Z. Phys. D* **2** (1986), 79.